FISEVIER

Contents lists available at ScienceDirect

Surface & Coatings Technology

journal homepage: www.elsevier.com/locate/surfcoat



Needle grass array of nanostructured nickel cobalt sulfide electrode for clean energy generation



Camila Zequine^a, Sanket Bhoyate^a, Khamis Siam^a, Pawan K. Kahol^b, Nikolaos Kostoglou^c, Christian Mitterer^c, Steven J. Hinder^d, Mark A. Baker^d, Georgios Constantinides^e, Claus Rebholz^f, Gautam Gupta^g, Xianglin Li^h, Ram K. Gupta^{a,*}

- ^a Department of Chemistry, Pittsburg State University, Pittsburg, KS 66762, USA
- ^b Department of Physics, Pittsburg State University, Pittsburg, KS 66762, USA
- ^c Department of Physical Metallurgy and Materials Testing, Montanuniversität Leoben, 8700 Leoben, Austria
- d Department of Mechanical Engineering Sciences, University of Surrey, GU2 7XH Guildford, UK
- e Department of Mechanical Engineering and Materials Science and Engineering, Cyprus University of Technology, 3036 Lemesos, Cyprus
- f Department of Mechanical and Manufacturing Engineering, University of Cyprus, 1678 Nicosia, Cyprus
- ⁸ Department of Chemical Engineering, University of Louisville, Louisville, KY 40292, USA
- ^h Department of Mechanical Engineering, University of Kansas, Lawrence, KS 66046, USA

ARTICLE INFO

Keywords: NiCo-OH $NiCo_2S_4$ OER HERWater electrolysis

ABSTRACT

Significant efforts have been focused on the search of earth-abundant elements to solve growing energy issues and to provide bifunctional behavior for both hydrogen and oxygen evolution reaction. Mixed transition metals could provide promising synergistic electrochemical properties and serve as bi-catalyst for overall water splitting process. In this study, a needle grass array of nanostructured nickel cobalt sulfide (NiCo₂S₄) was synthesized using a hydrothermal process. The synthesized NiCo₂S₄ electrodes showed promising electrocatalytic activity with a low overpotential of 148 mV and 293 mV for hydrogen and oxygen evolution reactions, respectively. The electrolyzer cell consisting of two NiCo₂S₄ electrodes displayed excellent performance with high electrochemical stability and low overall cell potential of 1.61 V to achieve a current density of 10 mA/cm². Our study suggests that mixed transition metal chalcogenides such as NiCo₂S₄ could be used as efficient and stable electrocatalyst for overall water splitting process.

1. Introduction

Out of humanity's ten problems addressed by Nobel Laureate Richard E. Smalley, "Energy" is top of the list [1]. Increasing energy demands, depletion of fossil fuels and growing environmental concerns are three major issues affecting the human society [2–4]. Current scientific and technological interest is focusing on using hydrogen as an efficient and carbon-free energy carrier and a potential transportation fuel [5]. Mass production of hydrogen is carried out using the steammethane reforming method, which evolves huge amounts of carbon dioxide into the atmosphere [5,6]. However, hydrogen production through water electrolysis, involving the hydrogen evolution reaction (HER), could serve as a cleaner way to produce hydrogen without any greenhouse emissions if the electricity needed for the electrolysis is provided by a renewable source. In addition, the oxygen evolution reaction (OER) serves as a key process for various energy conversion and

storage devices, including metal-air batteries, fuel cells, and electrolyzers [7,8]. The thermodynamic potential for the water splitting reaction is 1.23 V (vs. reverse hydrogen electrode, RHE), however, higher dynamic overpotentials limit the practicality of this process [9]. Some of the efficient benchmark electrocatalysts for OER includes ruthenium oxide (RuO2) and iridium oxide (IrO2), while for HER platinum (Pt) is most common [10]. Unfortunately, the applicability of these noblemetal based catalysts is limited due to lack of abundance, very high cost, stability issues, and poor integration of multifunctional behavior [9,11].

Recent advances have been made in developing earth-abundant transitional metal oxides, hydroxides, sulfides, phosphides, carbides and nitrides for energy conversion and storage devices [7–9,12–19]. Even though studies provide improved electrochemical activities of these materials for energy applications, bifunctionality (i.e., to be used for both OER and HER process) of the electroactive material still

E-mail addresses: rgupta@pittstate.edu, ramguptamsu@gmail.com (R.K. Gupta).

^{*} Corresponding author.

remains a challenge. Mixed valence oxides, hydroxides and sulfides based on Mn, Zn, Ni, Co and Fe, have recently attracted remarkable attention due to improved electrochemical properties and multifunctional uses for energy [8,9,19–25]. In particular, hydroxides and sulfides of Ni and Co are widely studied due to excellent electrochemical performance for different applications [14–16,26,27]. However, mixed compositions containing Ni and Co are known to have superior properties due to higher conductivity, electrochemical stability, and synergistic interactions [22,24,25,27]. Synergistically promoted kinetics on varied active sites, along with electronically reconfigured interfaces, provide eminent performance over single component energy generation or storage [6,9,20]. Moreover, a binderfree approach could eliminate the negative effects on stability and electrocatalytic activities observed in dip-coated samples [28,29].

Considering the importance of the aforementioned challenges, mixed transition metal hydroxide and sulfide, based on Ni and Co, were synthesized in the current work for bifunctional applicability such as electrocatalyst for OER and HER process. Nickel-cobalt hydroxide (NiCo-OH) and nickel-cobalt sulfide (NiCo_2S_4) were synthesized using a facile hydrothermal reaction. Direct growth of electroactive material over the Ni foam substrate showed higher electrochemical performance for energy generation. The electrocatalytic activity of the samples was characterized using OER and HER measurements in alkaline media. The electrolyzer device using NiCo_2S_4 both as anode and cathode showed low potential of 1.61 V to achieve a current density of $10 \, \text{mA/cm}^2$ with outstanding electrochemical stability.

2. Experimental details

NiCo-OH was synthesized using a facile hydrothermal method. In a typical synthesis, 125 mg of cobalt nitrate, 62.5 mg of nickel nitrate and 4 ml of glycerol were dissolved in 20 ml isopropanol to form a transparent pink solution. This solution was then transferred into a 45 ml Teflon autoclave reactor containing a pre-cleaned Ni foam. The reaction was carried out at 180 $^{\circ}$ C for 6 h. After cooling the reactor to room temperature, Ni foam deposited with NiCo-OH was washed several times with ethanol and dried under vacuum at 60 $^{\circ}$ C for 10 h.

NiCo₂S₄ was synthesized by sulfurizing the NiCo-OH coated Ni foam. For this conversion, the latter was placed into a Teflon reactor containing 50 mg of thioacetamide in 20 ml of ethanol. The sulfurization was carried out at 160 °C for 6 h. The obtained electrode was washed with ethanol and dried under vacuum at 60 °C for 10 h. The schematic for the synthesis procedure is given in Fig. 1. For comparison, cobalt hydroxide (Co(OH)2) and nickel hydroxide (NiOH) were synthesized on Ni foam using the above methods. Commercial IrO2 and platinum, for use as OER and HER electrocatalysts, were purchased from Alfa Aesar, and Sigma Aldrich, respectively. The NiCo-OH and NiCo₂S₄ samples were analyzed using X-ray diffraction (XRD), X-ray photoelectron spectroscopy (XPS), and scanning electron microscopy (SEM) combined with energy dispersive X-ray spectroscopy (EDS) to elucidate structural, chemical and morphological properties. XRD was performed over the scrap-out powder from the Ni foam electrode using a Shimadzu X-ray diffractometer (Lenexa, Kansas, USA) to study the phase purity of the synthesized samples. XRD patterns were recorded using $CuK\alpha_1$ radiation ($\lambda = 1.5406 \,\text{Å}$) in 2θ – θ mode. The microstructural and morphological characterestics of the NiCo-OH and NiCo₂S₄ films, hydrothermally deposited on Ni foams, were studied using a Quanta 200 SEM (FEI, Hillsboro, Oregon, USA) at an acceleration voltage of 20 kV. The samples were also micro-analyzed using the EDVAC Genesis X-ray analysis probe. The spectral patterns, that allowed elemental compositions as well as elemental mapping in space, were generated and recorded for each session. XPS analysis was performed over the scrap-out powder from the Ni foam electrode using a ThermoFisher Scientific Instruments K-Alpha+ spectrometer (East Grinstead, UK) to study the chemical composition of the synthesized samples. The XPS instrument was equipped with a monochromated Al

Kα radiation source (hν = 1486.6 eV) and an X-ray spot of ~400 μm in radius. Survey spectra were acquired with a pass energy of 200 eV, while high-resolution core level spectra for all elements were acquired with a pass energy of 50 eV. Quantitative chemical compositions were calculated from the high-resolution core level spectra following the removal of a non-linear Shirley background. The Avantage software was used for the peak fittings as it incorporates the appropriate sensitivity factors and corrects for the electron energy analyzer transmission function.

Electrochemical measurements were performed using a Versastat 4-500 electrochemical workstation (Princeton Applied Research, USA). The electrocatalytic performance of the electrodes was analyzed using a three-electrode system. A graphite rod was used as a counter electrode, a saturated calomel electrode (SCE) as a reference electrode, and the synthesized electrodes were used as working electrodes in 1 M KOH. Electrocatalytic testing included linear sweep voltammetry (LSV), cyclic voltammetry (CV) and chronoamperometry. LSV was performed at a scan rate of 1 mV/s for both OER and HER. The potential was converted to RHE using the Nernst equation [30]. Electrodes were also analyzed using electrochemical impedance spectroscopy (EIS) studies in a frequency range of 0.05 Hz to 10 kHz with an applied 10 mV of AC amplitude.

3. Results and discussion

XRD measurements were carried out to analyze the phase purity and crystalline nature of the synthesized samples. These studies were performed on the scraped powders from the Ni-foam. X-ray diffractograms of the synthesized samples are shown in Fig. 2. NiCo-OH sample showed diffraction peaks at 20 values of around 12.1°, 24.5°, 33.2° and 59.1°, which corresponds to the α -phase of nickel-cobalt double hydroxide. The X-ray diffractogram of the sulfurized nickel-cobalt double hydroxide matches with the NiCo₂S₄ phase. More specifically, all the diffraction peaks can be indexed to the cubic phase of NiCo₂S₄ (JCPDS card No. 43-1477) with no obvious oxide impurities, thus indicating a total conversion of nickel-cobalt double hydroxide to NiCo₂S₄. Both X-ray diffractograms match well with nickel cobalt hydroxide and nickel cobalt sulfide phases and are in accordance with literature reports [31–34].

Scanning electron microscopy was used to investigate the microstructure and morphology of the NiCo-OH and NiCo₂S₄. Fig. 3(a-c) show SEM images of the NiCo-OH at various magnifications. The surface of the Ni-foam was covered with NiCo-OH spheres with size ranging from 500 to 1500 nm. The spatial distribution of elements can be observed using EDS by acquiring the characteristic X-ray emission lines of Ni, Co, and O, as evidenced in Fig. S1. It becomes apparent that Ni is primarily concentrated within the substrate material while the spheres that cover most of the surface consist of Ni, Co and O, suggesting the correspondence with the crystalline phase of NiCo-OH detected through XRD. The morphology and structure of the sulfurized NiCo-OH specimen at various magnifications is shown in Fig. 3(d-f). It appears that the NiCo-OH nano-spheres convert into a dense film of a nanostructured needle-grass array of NiCo₂S₄ having needle diameters between 50 and 100 nm. The solid film layer has a thickness of approximately 2 µm, beyond which nano-needles protrude for another 1–2 µm (see Fig. 3(e)). Fig. S2 corresponds to the EDX elemental maps showing the uniform distribution of Ni, Co, S in accordance with the crystal structure of NiCo₂S₄ detected through XRD.

Fig. S3 shows the XPS survey-scan spectrum of the NiCo-OH and NiCo₂S₄ and confirms the presence of the expected elements [35]. The Ni and Co 2p core level spectra for the hydroxide are shown in Fig. S4(a) and Fig. S4(b), respectively. Both spectra show the presence of satellites associated with the $2p_{3/2}$ and $2p_{1/2}$ spin orbit split components. The binding energy of the Ni $2p_{3/2}$ peak occurs at 855.0 eV and the satellite at 861.3 eV. The binding energy of the Co $2p_{3/2}$ peak occurs at 780.3 eV and the satellite at 786.0 eV. For both Ni and Co, the

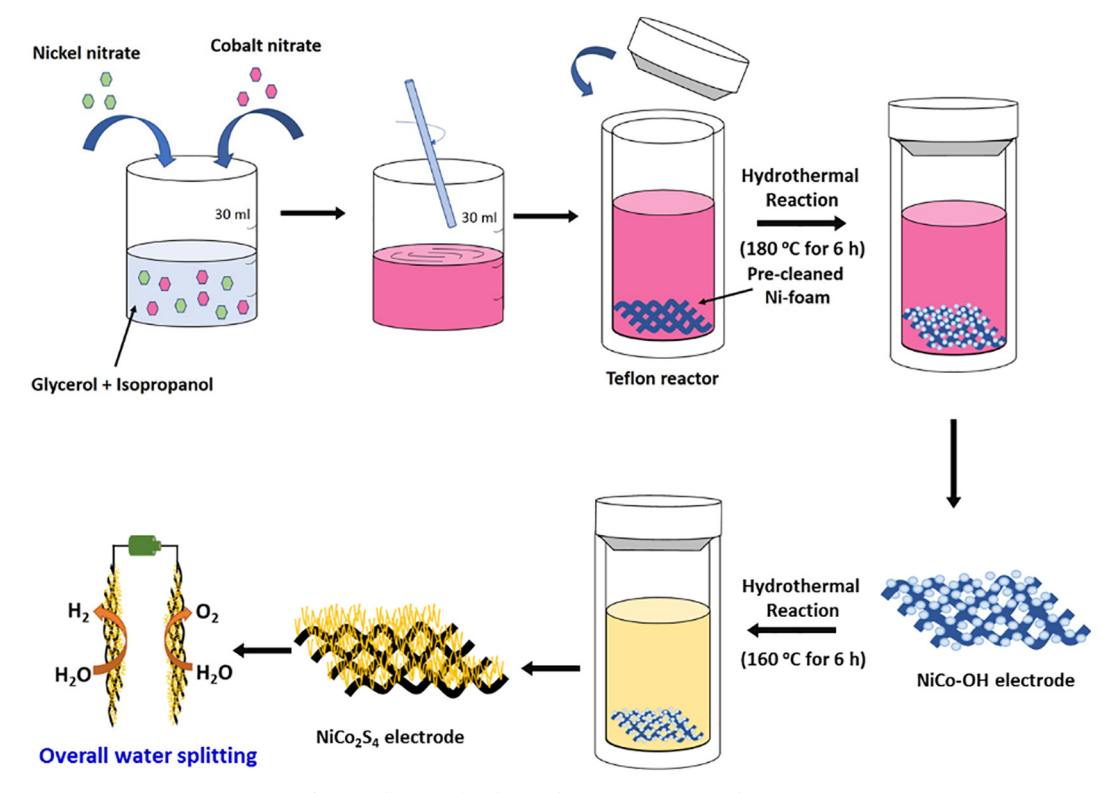
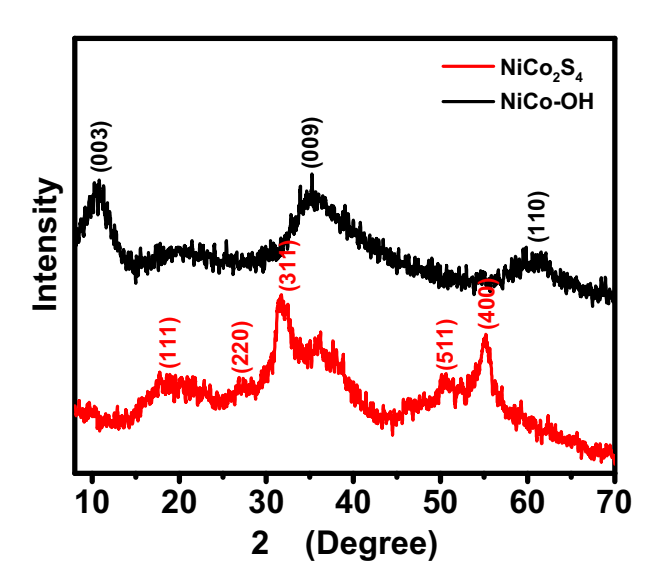


Fig. 1. Schematic for the synthesis of NiCo-OH and NiCo₂S₄.



 $\textbf{Fig. 2.} \ \textbf{X-ray diffractogram of the synthesized NiCo-OH and NiCo}_2S_4.$

binding energies and satellite structure indicate the probable presence of both metal (2+) hydroxides and metal (3+) oxyhydroxides [36,37]. The binding energy of the O 1s peak occurs at 530.7 eV, which sits between the expected binding energies of the metal oxides and hydroxides, which also supports the mix of metal 2+/3+ species in the NiCo hydroxide/oxyhydroxide formed. This mixed oxidation state is in agreement with the XRD assignment of a nickel-cobalt double hydroxide.

The Ni 2p, Co 2p and S 2p spectra for the NiCo sulfide (NiCo $_2$ S $_4$) are given in Fig. S4(c–e). The spectral shape for the Ni and Co 2p peak envelope is similar and corresponds to different Ni–S and Co–S species. To understand the physical interpretation of these peaks, it is pertinent to first look at the S 2p peak envelope, which is also quite complex. The largest S 2p component, with a binding energy of 169.1 eV and a

shoulder at 170.3 eV corresponds to the S 2p_{3/2} and S 2p_{1/2} peaks, respectively, for NiCo sulfate [38,39]. The lowest binding energy component at around 162.5 eV corresponds to the 2p3/2 peak for NiCo2S4 [40,41]. The larger and higher binding energy component at 163.7 eV has a binding energy typical of elemental sulfur [42] and a study of sulfide mineral surfaces suggests that a S 2p_{3/2} peak observed at binding energies of $163.0\text{--}164.2\,\text{eV}$ corresponds to the presence of elemental sulfur, rather than polysulfide or metal sulfide species (which occur at lower binding energies) [43]. Returning to the Ni 2p spectra, the components at approximately 854 and 857 eV correspond to the Ni 2p3/2 peaks for NiCo sulfide and NiCo sulfate, respectively, and the broader peak at around 862 eV is the Ni 2p3/2 satellite. There is the corresponding Ni $2p_{1/2}$ envelope for these components at higher binding energies. For the Co 2p spectra, there is a similar set of peaks to the Ni 2p, with the components at around 778 and 782 eV corresponding to the Co 2p3/2 peaks for NiCo sulfide and NiCo sulfate respectively together with the satellite peak at around 786 eV and the associated Co 2p_{1/2} peaks at higher binding energies. Hence, the surface of these NiCo2S4 needles is complex, with the presence of sulfide, sulfate and elemental sulfur species.

The electrocatalytic performance of NiCo-OH and NiCo₂S₄ as OER electrocatalysts was investigated using LSV. The polarization curves for all the synthesized samples, along with the commercial IrO₂, are shown in Fig. 4(a). NiCo-OH showed a lower overpotential (i.e. 339 mV) compared to its counter nickel hydroxide (i.e. 374 mV) and cobalt hydroxide (i.e. 351 mV) at a current density of 10 mA/cm². This could be due to mixed-composition metal hydroxide catalyst providing synergistic interactions and enhanced electrochemical performance [22–24,44,45]. Reports suggest further improvement in electrocatalytic performance for metal chalcogenides [9,16,46,47]. Hence, after sulfurization of NiCo-OH, the overpotential value reduced to 293 mV, which is better than the equivalent value of the commercial IrO2 catalyst (i.e. 301 mV). NiCo₂S₄ showed better or comparable results to that of many previously reported metal sulfides and mixed-transition metal sulfides. For example, Liu et al. synthesized cobalt-sulfide nanosheet films over titanium mesh as an electrocatalyst for oxygen evolution, and

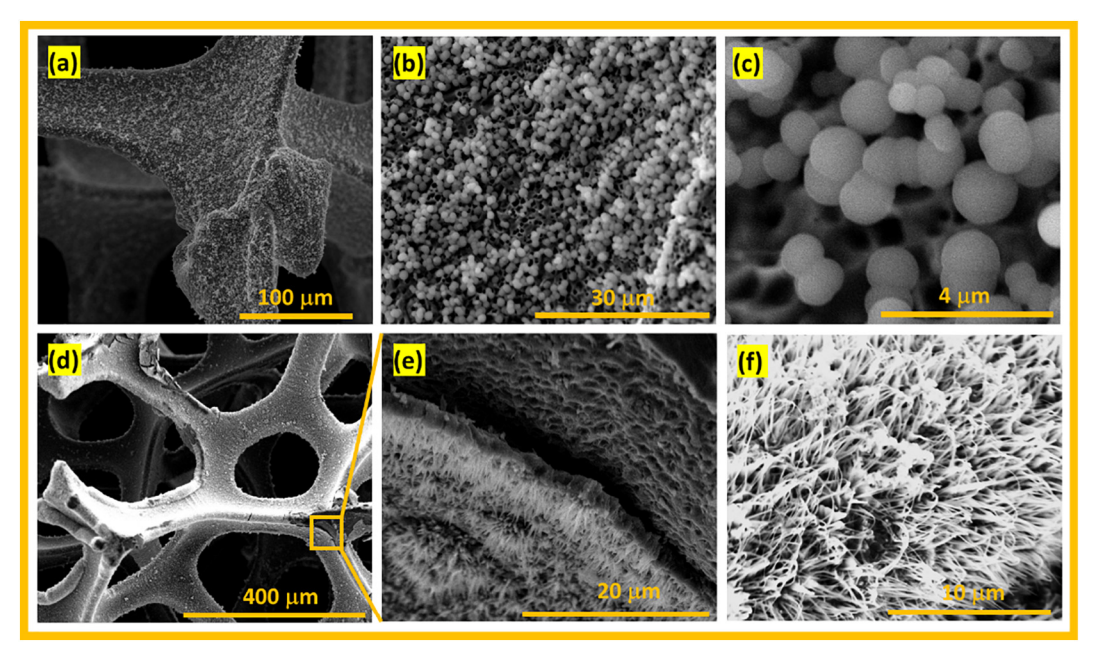


Fig. 3. SEM images for (a), (b), (c) NiCo-OH, and (d), (e), (f) NiCo₂S₄.

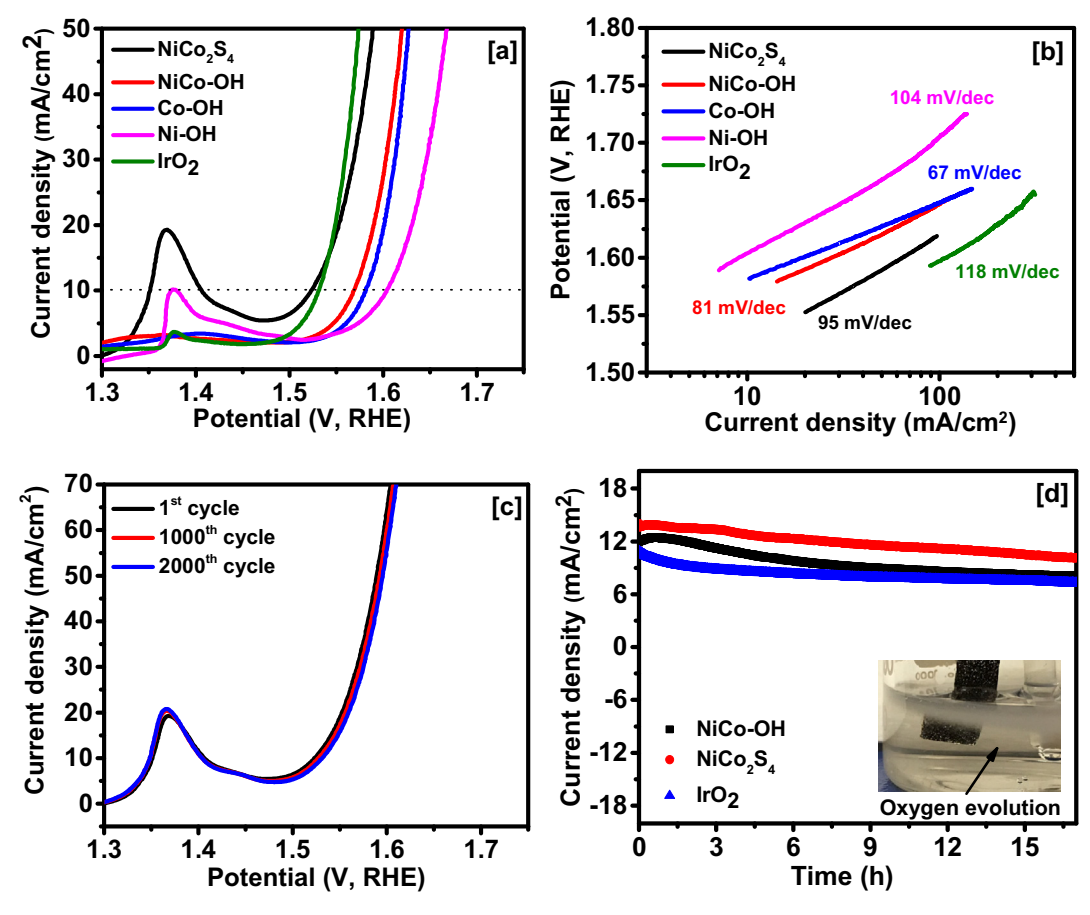


Fig. 4. OER results: (a) polarization curves, (b) Tafel slopes, (c) durability test of the $NiCo_2S_4$ electrocatalyst using LSV, and (d) stability performance of the electrodes using chronoamperometry (inset figure shows oxygen evolution during this experiment from the $NiCo_2S_4$ electrode).

observed an overpotential of 361 mV to obtain a current density of $10\,\text{mA/cm}^2$ [48]. Ren et al. synthesized hierarchical nickel sulfide nanosheets directly grown over Ni foam as an electrocatalyst for water reduction and oxidation [27]. Ni_3S_4 nanosheets directly grown over Ni foam delivered a current density of $20\,\text{mA/cm}^2$ for OER at the

overpotential of 320 mV. Whereas, mixed transition electrocatalysts synthesized by Chauhan et al. showed improved OER performance of CuCo_2S_4 (310 mV at $10\,\text{mA/cm}^2$) compared to ideal Co_3S_4 (> 450 mV at $10\,\text{mA/cm}^2$) [49]. The improved performance was attributed to the Cu^{2+} site for absorption of –OH, –O and –OOH reactive species. The

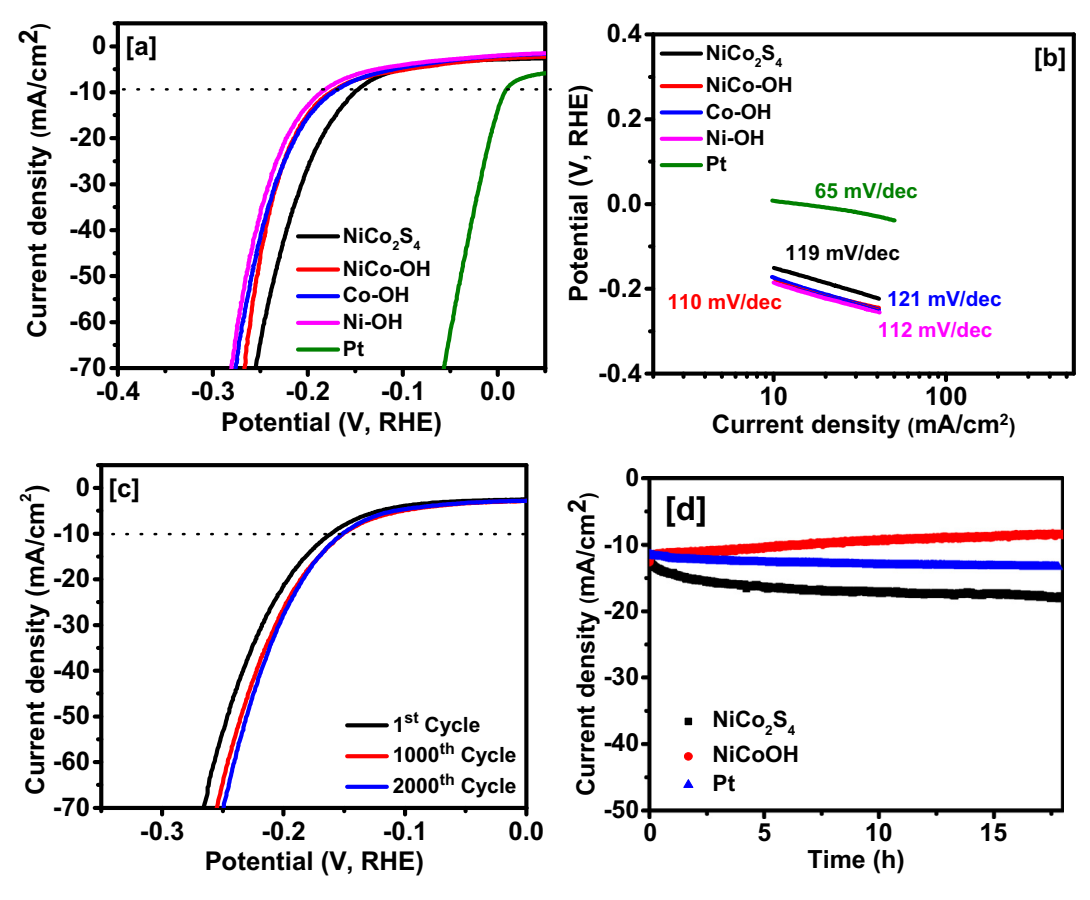


Fig. 5. HER results: (a) polarization curves, (b) Tafel slopes, (c) durability test of the NiCo₂S₄ electrocatalyst using LSV, and (d) stability performance of the electrodes using chronoamperometry.

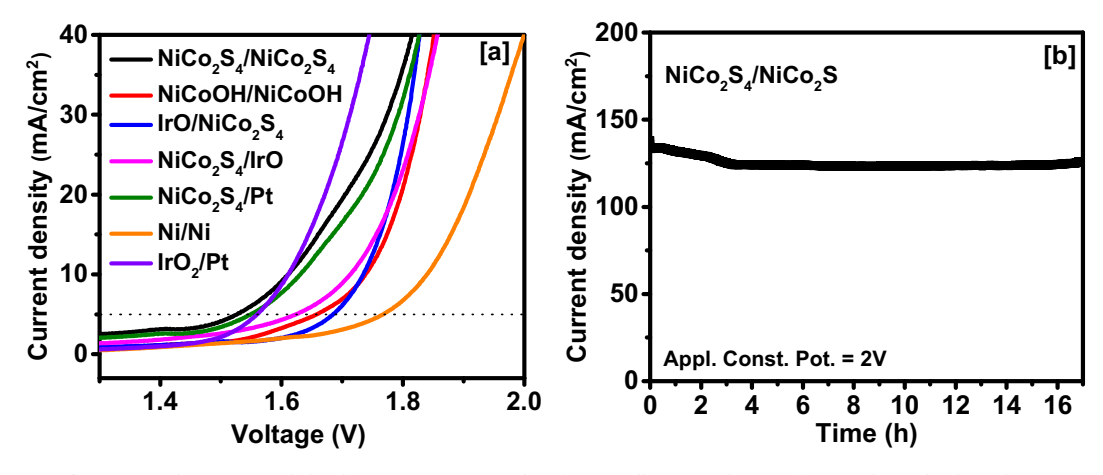


Fig. 6. (a) Polarization and (b) chronoamperometry plots for overall water splitting of a two-electrode electrolyzer.

series resistance of the synthesized samples at different potentials was analyzed using EIS (see Fig. S5). It is observed that charge transfer resistance of ${\rm NiCo_2S_4}$ is lower than that of NiCo-OH at same potentials. In addition to lower charge transfer resistance, ${\rm NiCo_2S_4}$ also displayed lower total impedance compared to NiCo-OH. The reduced series resistance of NiCo₂S₄ with increasing potential showed better catalytic performance over NiCo-OH. The electrochemically active surface area (ECSA) of NiCo-OH and NiCo₂S₄ was estimated using CV in the non-Faradic region. The cyclic voltammograms show typical rectangular like-shaped curves with no oxidation or reduction peaks, suggesting regular feature of electrical double layer capacitor (see Fig. S6). A linear relationship between current density and scan rate of the synthesized

samples was observed. The slope of these curves provide the value of double layer capacitance which is directly related to the surface area of these materials [50]. Double layer capacitance of 10.4 and 17.4 mF/cm² was calculated for NiCo-OH and NiCo $_2$ S $_4$, respectively. The Tafel slope indicates the reaction kinetics for the different catalysts (see Fig. 4(b)). Although NiCo $_2$ S $_4$ showed lower overpotential at 10 mA current, the kinetics of the reaction was observed to be little sluggish and close to other reports [6]. NiCo $_2$ S $_4$, NiCo-OH, Co-OH, NiOH and IrO $_2$ showed a Tafel slope of 95, 81, 67, 104 and 118 mV/dec, respectively. Table S1 shows a comparison for the OER performance of the synthesized catalysts with other previously reported results in alkaline media.

The durability of the NiCo₂S₄ electrode towards OER was investigated using cyclic stability tests and chronoamperometry. The polarization curves for NiCo₂S₄ showed the minimal difference of 10 mV after 2000 cycles (see Fig. 4(c)). The catalytic performance was also tested using chronoamperometry and compared with an IrO₂ catalyst. As observed from Fig. 4(d), the current density of NiCo₂S₄ remained almost constant for $>17\,h$ of testing. From the overall measurements, it was observed that NiCo₂S₄ exhibits a stable and durable catalytic performance, comparable to the commercial catalyst, and has the potential to be used as a highly efficient OER catalytic electrode.

The electrochemical performance of NiCo-OH and NiCo₂S₄ as HER electrocatalysts was also investigated. Fig. 5(a) shows the polarization curves for all the tested samples. NiCo₂S₄ showed an overpotential of 148 mV, which is much lower than that for NiCo-OH (i.e. 170 mV), Co-OH (i.e. 173 mV), and Ni-OH (i.e. 185 mV) to deliver a current density of 10 mA/cm². The needle grass arrays of NiCo₂S₄ synthesized in this work outperformed other metal sulfides and mixed-transition metal catalysts. For example, a case study of crystalline NiS, NiS2 and Ni3S2 nanoparticles showed overpotentials of 474, 454 and 355 mV, respectively [51]. Irshad et al. synthesized honey-comb structured NiCo₂S₄ as a HER catalyst, using an electrochemical deposition method and required a high overpotential of 280 mV (at 10 mA/cm²) [6]. Huang et al. synthesized Co-doped iron sulfide as an electrocatalyst for HER [52]. The overpotential required to drive 10 mA/cm2 was 150 mV and showed a decrease of 1 mV after 500 cycles. As shown in Fig. 5(b), Tafel slope for NiCo₂S₄, NiCo-OH, Co-OH, Ni-OH and Pt were calculated to be 119, 110, 121, 112 and 65 mV/dec, respectively. The obtained results for NiCo-OH and NiCo₂S₄ are comparable to other noble metal-free HER electrocatalysts (see Table S2).

The durability of the NiCo₂S₄ electrode as a HER electrocatalyst was analyzed using cyclic stability tests and chronoamperometry. After 2000 cycles, NiCo₂S₄ showed a reduced overpotential of 10 mV at 10 mA/cm², as seen in Fig. 5(c). A similar behavior was also observed in the chronoamperometric measurements, as seen in Fig. 5(d). The performance of the NiCo₂S₄ electrode improved over a period of time at a constant potential. The aformentioned results suggest that NiCo₂S₄ can be used as a durable electrocatalyst for HER processes.

Catalytic activities of different electrodes were tested by fabricating an electrolyzer for overall water splitting, and the polarization curves for various combinations are shown in Fig. 6(a). The potential obtained for the NiCo₂S₄/NiCo₂S₄, as a symmetrical catalytic electrode system, showed better values among all the different combinations tested with the aim to understand the performance of NiCo₂S₄ in detail. Specifically, the NiCo₂S₄/NiCo₂S₄ device required an onset potential of 1.46 V. A current density of $10\,\text{mA/cm}^2$ was obtained at $1.61\,\text{V}$ for the NiCo₂S₄/NiCo₂S₄ device, while the same potential was required for the IrO₂(anode)/Pt (cathode) device.

IrO2(anode)/NiCo2S4(cathode), Moreover. IrO₂(cathode)/ NiCo₂S₄(anode) and NiCo₂S₄(anode)/Pt(cathode) devices required 1.71, 1.64 and 1.63 V, respectively, to achieve a current density of 10 mA/cm². The NiCo₂S₄/NiCo₂S₄ device showed a comparable performance to other two-electrode systems reported within the literature (see Table S3). The chronometric response of the NiCo2S4/NiCo2S4 and NiCo-OH/NiCo-OH system is shown in Fig. S7, with the NiCo₂S₄/ NiCo₂S₄ device displaying a very stable performance over an extended period of time. In practice, the electrolysis is carried out at higher potentials. Hence, the stability of the electrolyzer was studied at a higher current density by applying a constant potential of 2 V to the NiCo₂S₄/ NiCo₂S₄ electrolyzer (Fig. 6(b)). The aformentioned studies on a device basis showed that the NiCo₂S₄/NiCo₂S₄ electrolyzer maintained a stable performance over a period of 17 h, thus indicating superior stability of the synthesized electrodes.

4. Conclusion

The current work demonstrated that mixed transition metal

chalcogenides such as $NiCo_2S_4$ could be used for energy generation via electrocatalysis. The $NiCo_2S_4$ outperformed both the NiCo-OH and the individual hydroxides as a water-splitting electrocatalyst. Moreover, the electrodes showed a superior stability performance for both OER and HER reactions for up to 2000 cycles. Symmetrical electrode cell of $NiCo_2S_4$ required a low potential of 1.61 V to achieve a current density of $10\,\text{mA/cm}^2$. The findings of this study suggest that $NiCo_2S_4$ electrodes can be used effectively for energy generation as efficient electrocalatyst for overall water splitting process.

Author contributions

RKG conceived the project, designed the experiments, interpreted the data, and finalized the manuscript. First draft of the manuscript was written by CZ and SB. CZ and SB performed all the electrochemical measurements and recorded the XRD data. GC provided SEM images and analysis. MB and SH provided XPS data and analysis. All authors reviewed and commented on the manuscript.

Acknowledgments

Dr. Ram K. Gupta expresses his sincere acknowledgment to the Polymer Chemistry Program and Kansas Polymer Research Center, Pittsburg State University for providing financial and research support to complete this project. Financial support by the Austrian Federal Government (in particular from Bundesministerium für Verkehr, Innovation und Technologie and Bundesministerium für Wissenschaft, Forschung und Wirtschaft) represented by Österreichische Forschungsförderungsgesellschaft mbH and the Styria and the Tyrolean Provincial Government, represented by Steirische Wirtschaftsförderungsgesellschaft mbH and Standortagentur Tirol, within the framework of the COMET Funding Programme is gratefully acknowledged by NK and CM. XL wants to thank the financial support from New Faculty General Research Fund, General Research Fund provided by the University of Kansas and funding support from NSF (1833048).

Appendix A. Supplementary data

Supplementary data to this article can be found online at https://doi.org/10.1016/j.surfcoat.2018.09.045.

References

- J. Wu, Z. Lan, J. Lin, M. Huang, Y. Huang, L. Fan, G. Luo, Electrolytes in dyesensitized solar cells, Chem. Rev. 115 (2015) 2136.
- 2] A. Witze, That's oil, folks..., Nature 445 (2007) 14.
- [3] M.S. Dresselhaus, I.L. Thomas, Alternative energy technologies, Nature 414 (2001) 332.
- [4] A.Y. Hoekstra, T.O. Wiedmann, Humanity's unsustainable environmental footprint, Science 344 (2014) 1114.
- [5] W. Lubitz, W. Tumas, Hydrogen: an overview, Chem. Rev. 107 (2007) 3900.
- [6] A. Irshad, N. Munichandraiah, Electrodeposited nickel-cobalt-sulfide catalyst for the hydrogen evolution reaction, ACS Appl. Mater. Interfaces 9 (2017) 19746.
- [7] W. Zhang, W. Lai, R. Cao, Energy-related small molecule activation reactions: oxygen reduction and hydrogen and oxygen evolution reactions catalyzed by porphyrin- and corrole-based systems, Chem. Rev. 117 (2017) 3717.
- [8] Q. Zhao, Z. Yan, C. Chen, J. Chen, Spinels: controlled preparation, oxygen reduction/evolution reaction application, and beyond, Chem. Rev. 117 (2017) 10121.
- [9] Y. Yang, K. Zhang, H. Lin, X. Li, H.C. Chan, L. Yang, Q. Gao, MoS₂–Ni₃S₂ heteronanorods as efficient and stable bifunctional electrocatalysts for overall water splitting, ACS Catal. 7 (2017) 2357.
- [10] Y. Pei, Y. Yang, F. Zhang, P. Dong, R. Baines, Y. Ge, H. Chu, P.M. Ajayan, J. Shen, M. Ye, Controlled electrodeposition synthesis of Co-Ni-P film as a flexible and inexpensive electrode for efficient overall water splitting, ACS Appl. Mater. Interfaces 9 (2017) 31887.
- [11] X. Zou, Y. Zhang, Noble metal-free hydrogen evolution catalysts for water splitting, Chem. Soc. Rev. 44 (2015) 5148.
- [12] C.K. Ranaweera, C. Zhang, S. Bhoyate, P.K. Kahol, M. Ghimire, S.R. Mishra, F. Perez, B.K. Gupta, R.K. Gupta, Flower-shaped cobalt oxide nano-structures as an efficient, flexible and stable electrocatalyst for the oxygen evolution reaction, Mater. Chem. Front. 1 (2017) 1580.

- [13] C. Zhang, Z. Wang, S. Bhoyate, T. Morey, B. Neria, V. Vasiraju, G. Gupta, S. Palchoudhury, P. Kahol, S. Mishra, F. Perez, R. Gupta, MoS₂ Decorated Carbon Nanofibers as Efficient and Durable Electrocatalyst for Hydrogen Evolution Reaction, C 3 (2017), p. 33.
- [14] M. Gong, W. Zhou, M.-C. Tsai, J. Zhou, M. Guan, M.-C. Lin, B. Zhang, Y. Hu, D.-Y. Wang, J. Yang, S.J. Pennycook, B.-J. Hwang, H. Dai, Nanoscale nickel oxide/nickel heterostructures for active hydrogen evolution electrocatalysis, Nat. Commun. 5 (2014) 4695.
- [15] M. Gong, D.Y. Wang, C.C. Chen, B.J. Hwang, H. Dai, A mini review on nickel-based electrocatalysts for alkaline hydrogen evolution reaction, Nano Res. 9 (2016) 28.
- [16] P. Ganesan, M. Prabu, J. Sanetuntikul, S. Shanmugam, Cobalt sulfide nanoparticles grown on nitrogen and sulfur codoped graphene oxide: an efficient electrocatalyst for oxygen reduction and evolution reactions, ACS Catal. 5 (2015) 3625.
- [17] B. You, N. Jiang, M. Sheng, M.W. Bhushan, Y. Sun, Hierarchically porous urchinlike Ni₂P superstructures supported on nickel foam as efficient bifunctional electrocatalysts for overall water splitting, ACS Catal. 6 (2016) 714.
- [18] J. Tian, Q. Liu, A.M. Asiri, X. Sun, Self-supported nanoporous cobalt phosphide nanowire arrays: an efficient 3D hydrogen-evolving cathode over the wide range of pH 0–14, J. Am. Chem. Soc. 136 (2014) 7587.
- [19] L. Trotochaud, S.L. Young, J.K. Ranney, S.W. Boettcher, Nickel-Iron oxyhydroxide oxygen-evolution electrocatalysts: the role of intentional and incidental iron incorporation, J. Am. Chem. Soc. 136 (2014) 6744.
- [20] L. Wang, X. Jiao, P. Liu, Y. Ouyang, X. Xia, W. Lei, Q. Hao, Self-template synthesis of yolk-shelled NiCo₂O₄ spheres for enhanced hybrid supercapacitors, Appl. Surf. Sci. 427 (2018) 174.
- [21] Y. He, L. Xu, Y. Zhai, A. Li, X. Chen, A hexangular ring-core NiCo₂O₄ porous nanosheet/NiO nanoparticle composite as an advanced anode material for LIBs and catalyst for CO oxidation applications, Chem. Commun. 51 (2015) 14768.
- [22] A. Balram, H. Zhang, S. Santhanagopalan, Enhanced oxygen evolution reaction electrocatalysis via electrodeposited amorphous α-phase nickel-cobalt hydroxide nanodendrite forests, ACS Appl. Mater. Interfaces 9 (2017) 28355.
- [23] H. Shi, G. Zhao, Water oxidation on spinel NiCo₂O₄ nanoneedles anode: micro-structures, specific surface character, and the enhanced electrocatalytic performance, J. Phys. Chem. C 118 (2014) 25939.
- [24] H. Ma, J. He, D.B. Xiong, J. Wu, Q. Li, V. Dravid, Y. Zhao, Nickel cobalt hydroxide @reduced graphene oxide hybrid nanolayers for high performance asymmetric supercapacitors with remarkable cycling stability, ACS Appl. Mater. Interfaces 8 (2016) 1992.
- [25] X. Li, Q. Li, Y. Wu, M. Rui, H. Zeng, Two-dimensional, porous nickel-cobalt sulfide for high-performance asymmetric supercapacitors, ACS Appl. Mater. Interfaces 7 (2015) 19316.
- [26] S. Chen, J. Zhu, X. Wang, One-step synthesis of graphene cobalt hydroxide nanocomposites and their electrochemical properties, J. Phys. Chem. C 114 (2010) 11829.
- [27] J.T. Ren, Z.Y. Yuan, Hierarchical nickel sulfide nanosheets directly grown on Ni foam: a stable and efficient electrocatalyst for water reduction and oxidation in alkaline medium, ACS Sustain. Chem. Eng. 5 (2017) 7203.
- [28] C. Yuan, H. Bin Wu, Y. Xie, X.W.D. Lou, Mixed transition-metal oxides: design, synthesis, and energy-related applications, Angew. Chem. Int. Ed. 53 (2014) 1488.
- [29] C.K. Ranaweera, C. Zhang, S. Bhoyate, P.K. Kahol, M. Ghimire, S.R. Mishra, F. Perez, B.K. Gupta, R.K. Gupta, Flower-shaped cobalt oxide nano-structures as an efficient, flexible and stable electrocatalyst for the oxygen evolution reaction, Mater. Chem. Front. 1 (2017) 1580.
- [30] H. Wang, H.-W. Lee, Y. Deng, Z. Lu, P.-C. Hsu, Y. Liu, D. Lin, Y. Cui, Bifunctional non-noble metal oxide nanoparticle electrocatalysts through lithium-induced conversion for overall water splitting, Nat. Commun. 6 (2015) 7261.
- [31] C. Nethravathi, N. Ravishankar, C. Shivakumara, M. Rajamathi, Nanocomposites of α-hydroxides of nickel and cobalt by delamination and co-stacking: enhanced stability of α-motifs in alkaline medium and electrochemical behaviour, J. Power Sources 172 (2007) 970.
- [32] C. Wang, X. Zhang, Z. Xu, X. Sun, Y. Ma, Ethylene glycol intercalated cobalt/nickel

- layered double hydroxide nanosheet assemblies with ultrahigh specific capacitance: structural design and green synthesis for advanced electrochemical storage, ACS Appl. Mater. Interfaces 7 (2015) 19601.
- [33] Y. Huang, T. Shi, S. Jiang, S. Cheng, X. Tao, Y. Zhong, G. Liao, Z. Tang, Enhanced cycling stability of NiCo₂S₄@NiO core-shell nanowire arrays for all-solid-state asymmetric supercapacitors, Sci. Rep. 6 (2016) 38620.
- [34] D.-Y. Kim, G.S. Ghodake, N.C. Maile, A.A. Kadam, D. Sung Lee, V.J. Fulari, S.K. Shinde, Chemical synthesis of hierarchical NiCo₂S₄ nanosheets like nanostructure on flexible foil for a high performance supercapacitor, Sci. Rep. 7 (2017) 0764
- [35] M. Yan, Y. Yao, J. Wen, L. Long, M. Kong, G. Zhang, X. Liao, G. Yin, Z. Huang, Construction of a hierarchical NiCo₂S₄@PPy core-shell heterostructure nanotube array on Ni foam for a high-performance asymmetric supercapacitor, ACS Appl. Mater. Interfaces 8 (2016) 24525.
- [36] A.P. Grosvenor, M.C. Biesinger, R.S.C. Smart, N.S. McIntyre, New interpretations of XPS spectra of nickel metal and oxides, Surf. Sci. 600 (2006) 1771.
- [37] J. Yang, H. Liu, W.N. Martens, R.L. Frost, Synthesis and characterization of cobalt hydroxide, cobalt oxyhydroxide, and cobalt oxide nanodiscs, J. Phys. Chem. C 114 (2010) 111.
- [38] V.I. Nefedov, A comparison of results of an ESCA study of nonconducting solids using spectrometers of different constructions, J. Electron Spectrosc. Relat. Phenom. 25 (1982) 29.
- [39] T.I. Korányi, I. Manninger, Z. Paál, O. Marks, J.R. Günter, Activation of unsupported Co-Mo catalysts in thiophene hydrodesulfurization, J. Catal. 116 (1989) 422
- [40] H. van der Heide, R. Hemmel, C.F. van Bruggen, C. Haas, X-ray photoelectron spectra of 3d transition metal pyrites, J. Solid State Chem. 33 (1980) 17.
- [41] H.W. Nesbitt, D. Legrand, G.M. Bancroft, Interpretation of Ni2p XPS spectra of Ni conductors and Ni insulators, Phys. Chem. Miner. 27 (2000) 357.
- [42] B.J. L., K. H., G. J., U. G., A. F., C. N., K. Siegbahn, Molecular spectroscopy by means of ESCA II. Sulfur compounds. Correlation of electron binding energy with structure, Phys. Scr. 1 (1970) 286.
- [43] S.R. St. C., S.W. M., G.A. R., XPS of sulphide mineral surfaces: metal-deficient, polysulphides, defects and elemental sulphur, Surf. Interface Anal. 28 (1999) 101.
- [44] L. Shen, L. Yu, X.-Y. Yu, X. Zhang, X.W.D. Lou, Self-templated formation of uniform NiCo₂O₄ hollow spheres with complex interior structures for lithium-ion batteries and supercapacitors, Angew. Chem. Int. Ed. 54 (2015) 1868.
- [45] P. Bhojane, S. Sen, P.M. Shirage, Enhanced electrochemical performance of mesoporous NiCo₂O₄ as an excellent supercapacitive alternative energy storage material, Appl. Surf. Sci. 377 (2016) 376.
- [46] A.F. Gullá, L. Gancs, R.J. Allen, S. Mukerjee, Carbon-supported low-loading rhodium sulfide electrocatalysts for oxygen depolarized cathode applications, Appl. Catal. A Gen. 326 (2007) 227.
- [47] U.K. Sultana, T. He, A. Du, A.P. O'Mullane, An amorphous dual action electrocatalyst based on oxygen doped cobalt sulfide for the hydrogen and oxygen evolution reactions. RSC Adv. 7 (2017) 54995.
- [48] T. Liu, Y. Liang, Q. Liu, X. Sun, Y. He, A.M. Asiri, Electrodeposition of cobalt-sulfide nanosheets film as an efficient electrocatalyst for oxygen evolution reaction, Electrochem. Commun. 60 (2015) 92.
- [49] M. Chauhan, K.P. Reddy, C.S. Gopinath, S. Deka, Copper cobalt sulfide nanosheets realizing a promising electrocatalytic oxygen evolution reaction, ACS Catal. 7 (2017) 5871.
- [50] C.C.L. McCrory, S. Jung, J.C. Peters, T.F. Jaramillo, Benchmarking heterogeneous electrocatalysts for the oxygen evolution reaction, J. Am. Chem. Soc. 135 (2013) 16977.
- [51] N. Jiang, Q. Tang, M. Sheng, B. You, D. Jiang, Y. Sun, Nickel sulfides for electrocatalytic hydrogen evolution under alkaline conditions: a case study of crystalline NiS, NiS₂, and Ni₂S₂ nanoparticles, Catal. Sci. Technol. 6 (2016) 1077.
- [52] S.-Y. Huang, D. Sodano, T. Leonard, S. Luiso, P.S. Fedkiw, Cobalt-doped iron sulfide as an electrocatalyst for hydrogen evolution, J. Electrochem. Soc. 164 (2017) 276.